EARTH OBSERVATION AND GEOMATICS ENGINEERING
website: https://eoge.ut.ac.ir

Temporal and Spatial Heat Island Pattern Investigation of 20 Different Regions over the World with Different Weather Conditions

Ramin Mokhtari-Dehkordi, Zeinab Akhavan, Reza Shah-Hosseini*

School of Surveying and Geospatial Engineering, College of Engineering, University of Tehran, Tehran, Iran

Article history:
Received: 24 February 2020, Received in revised form: 19 January 2021, Accepted: 6 February 2021

ABSTRACT

The surface temperature is an essential parameter in controlling and evaluating the physical and chemical processes of the surface of the earth. The Surface Urban Heat Island (SUHI) is the difference in temperature between urban and suburban areas. This study aims to consider the heat island of the urban and suburban areas of 20 different regions in the world with different weather conditions. In order to calculate the surface temperature of the earth in the daytime, the segmentation of the urban and suburban areas and the acquisition of several spectral indices from the Landsat 8 data were used. To calculate the surface temperature of the earth at night, at the same time as Landsat 8 data acquisition at daytime, an Eight-day product of the Earth's surface temperature MODIS (MOD11A21) was used. Land Surface Temperature (LST) of Landsat 8 images was calculated using a split-window algorithm. The results of this study indicate that the heat island of the urban area varies from one region to another. For most of the Mediterranean and temperate regions, the SUHI was positive for both day and nighttimes. For the warm, dry, and desert weather conditions the SUHI was positive at night and negative at daytime. Just for Manama city, the SUHI was negative at night and positive at daytime. However, the positive or negative value of this phenomenon in these twenty regions has been stable over two study time. Also, the effect of spectral indices on this phenomenon was measured. The GVI vegetation index's correlation coefficient was calculated to be -0.823, and the IBI Built-Up Index's correlation coefficient was calculated as 0.761.

KEYWORDS

SUHI

UHI

Urban and Sub-Urban areas

LST

Landsat8

MODIS

1. Introduction

Recently, the growth of the population and consequently, the expansion of urban areas in the world have led to changes in the patterns of the environment which is a result of the conversion of natural surfaces into artificial surfaces (Kalnay & Cai,2003). Due to the structure of impenetrable surfaces in urban areas, we are faced with a phenomenon called urban heat island. The difference in thermal characteristics of the urban and its surrounding regions creates a phenomenon in which urban areas have a higher temperature than their surroundings (Rizwan, Dennis & Chunho, 2008). Owing to this impenetrable structure of the urban regions, radiation that is entering urban areas will be trapped and have a reflection at night. As a result, the natural process of cooling down the ground at night will occur at a lower rate. Comparatively, non-urban areas are covered with vegetation and soil, and there are no rigid bodies such as buildings, so the evapotranspiration causes cooling of the non-urban surface areas (Wu & Zhang, 2018). The urban heat island phenomenon has been evaluated in different scenarios, including different geographical regions, times, seasons, and various sensors (Wang, Zhan & Guo,2016). According to prior studies, vegetation and the albedo coefficient increment of the surface, as well as population reduction in urban areas, can reduce the surface heat island in urban regions (Zhou et al.,2019). Investigating the changes in the temperature of the surface of the earth and the heat island has shown that as a result of the vegetation destruction inside and around cities, a very cold temperature (25-29 ° C) was replaced by an average temperature class (37-33° C). Also, by manipulating the sub-urban areas, their temperature rises to warm (37- 41

* Corresponding author

E-mail addresses: ramin.mokhtari.d@ut.ac.ir (Ramin Mokhtari Dehkordi); zeinab.akhavan.h@ut.ac.ir (Zeinab Akhavan Hamzeh); rshahosseini@ut.ac.ir (Reza Shah-hosseini)

DOI: 10.22059/eoge.2021.298383.1077

° C) and very hot temperatures (45-41 ° C). Time, wind speed, cloud cover, relative humidity, soil moisture, and snow are useful parameters on the intensity of the urban heat island, and the magnitude of this intensity depends on the season and the time of the day. Seasonally, the severity of the heat island of the urban areas is much higher in hot seasons than in cold seasons (Schatz & Kucharik, 2014). The reason that the magnitude of SUHI is affected by the changes in seasons is the changes in the intensity of the sun's radiation, land cover, and type of weather (Meng et al., 2018). According to these changes generally, the summer has the highest amount of SUHI (Ferguson et al., 2008). Urban Heat Island (UHI) is the difference in temperature between urban and surrounding areas, which is generally higher in urban areas at night. However, some exceptions can be observed in areas like Las Vegas and Madrid (Koken et al., 2003; Xian & Crane, 2006). In some cases, the purpose of studying UHI has been to focus on the growth of urban development and the way it affects this phenomenon. The results have shown that by urban development, the UHI has also increased (Sobrino et al., 2013). In some cases, the effect of vegetation and park increment on this phenomenon has been considered (Benas, Chrysoulakis & Cartalis, 2017), (Liu, Lau, Qin & Gou, 2017). In other studies, the effects of day and night have been evaluated on this phenomenon (Azevedo, Chapman & Muller, 2016). Urban Heat Island could have negative and destructive effects on human health, climate, and air quality (Debbege & Shepherd, 2015).

In this study, the SUHI of twenty different regions over the world has been studied. For each city, four SUHI have been calculated in hot and cold seasons. Landsat 8 images were taken for the day, and the eight-day product of Modis Earth surface temperature data was used for the night. The case studies have different types of climate, such as mountainous, tropical, Mediterranean, etc., which contains most of the climate types. One of the most important parameters that influence the heat island is the precise separation of urban from the sub-urban and surrounding areas.

2. The Proposed Method

In this study, to investigate the effects of time and place on heat islands, 20 urban areas from all over the world have been selected with different weather conditions.

2.1. Case Study

In this study, the cases for the study are 20 regions worldwide. The locations of these regions have been shown in Figure.1.

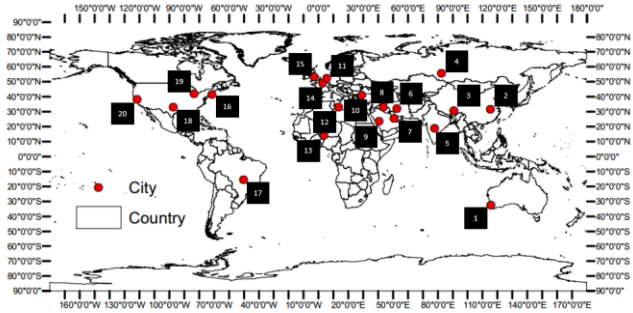

1	**Perth**	**11**	**Amsterdam**
2	**Wuhan**	**12**	**Tripoli**
3	**Lhasa**	**13**	**Niamey**
4	**Novosibrisk**	**14**	**Paris**
5	**Hyderabad**	**15**	**Liverpool**
6	**Isfahan**	**16**	**Boston**
7	**Manama**	**17**	**Brasilia**
8	**Baghdad**	**18**	**Dallas**
9	**Medina**	**19**	**Chicago**
10	**Istanbul**	**20**	**San Francisco**

Figure 1. Case Studies over the world

2.2. Data acquisition and preprocessing

2.2.1. Landsat Data

In this study, Landsat 8 images were used for calculation of the land surface temperature during the day, the classification of earth's surface in case studies, the segmentation of the urban area and its suburbs, and the acquisition of several spectral indices. Landsat 8 is an American Earth observation satellite launched on February 11, 2013. It is the eighth satellite in the Landsat program (He, Zhao, Li, Wen & Yu, 2019). Landsat Data for each region have been taken at two different times (Summer and Winter).

2.2.1. MODIS Data

To calculate the land surface temperature of the earth at the same time as Landsat data acquisition for all the case studies, the same eight-day product of the MODIS land surface temperature (MOD11A2) was used. The spatial resolution of MODIS data is 1km.

2.3. Methodology

Landsat 8 images were used for the separation of urban areas from surrounding areas and also LST calculation of the area during the day, as well as obtaining several spectral indices at two different times. For obtaining the land surface temperature of the earth at night, the land surface temperature of the MODIS eight-day product was used (Feng, Li, Tong, Chen & Liu, 2018). Figure.2 shows the flowchart of this study.

2.3.1. DN to Spectral Radiance Conversion

The spectral radiation of TIRS bands (10, 11 separately) was estimated by Eq. (1). Eq. (1) converts DN image to spectral radiance image.

$$L_\lambda = \left(\frac{L_{\max} - L_{\min}}{DN_{\max}} \right) * Band + L_{\min} \quad (1)$$

L_λ:Top of atmospheric spectral radiance in $watts / \left(m^2 \times srad \times \mu m \right)$

$L_{\max}$: Maximum spectral radiance of thermal (10, 11) bands

$DN_{\max}$: Difference of maximum and minimum calibration of the sensor

2.3.2. Brightness Temperature

To calculate the brightness temperature of bands 10 and 11, the spectral radiance of two thermal bands obtained from the previous step was converted to brightness temperature using Eq. (2).

$$TB = K2 / \left(\ln \left(\frac{K1}{L_\lambda} + 1 \right) \right) - 273{,}15 \quad (2)$$

K1, K2: Thermal constant values of bands 10 and 11 from the metadata file

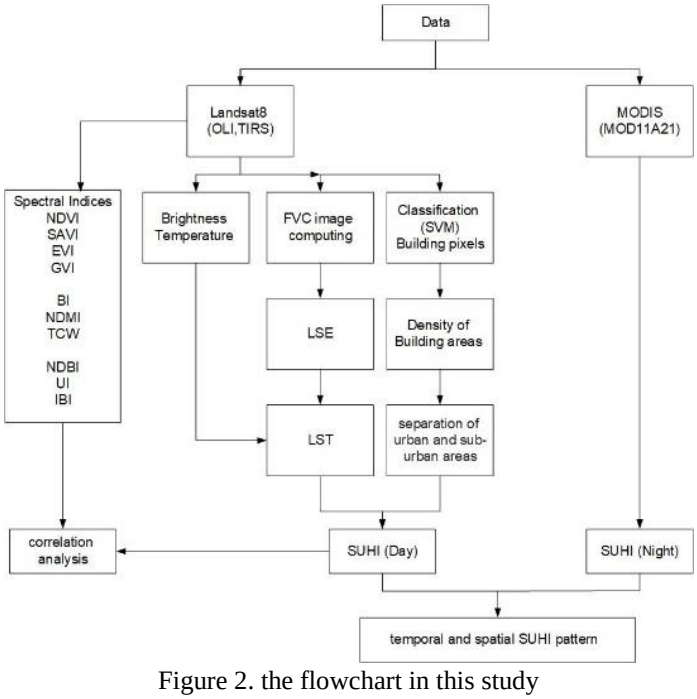

Figure 2. the flowchart in this study

2.3.2. Normalized Difference Vegetation Index

NDVI by optical bands 4 and 5 of the OLI sensor was estimated from a combination of bands 4 and 5 according to Eq. (3):

$$NDVI = \frac{Band_5 - Band_4}{Band_5 + Band_4} \quad (3)$$

$$-1 < NDVI < +1$$

2.3.4. Normalized Difference Vegetation Index

The FVC image obtained from the NDVI image was acquired using a part of the vegetation-covered area from Eq. (3). The split window algorithm uses the FVC image to estimate the LSE image. The NDVI image was classified into soil and vegetation classes, and the NDVI values were calculated separately for soil and vegetation. The FVC image was calculated by Eq. (4):

$$FVC = \frac{NDVI - NDVI\left(soil\right)}{NDVI\left(vegetation\right) - NDVI\left(soil\right)} \quad (4)$$

$$FVC = \frac{NDVI - 0.15}{0.48 - 0.15}$$

2.3.5. LSE Image Generated from FVC Image

The LSE image generated from the FVC image of the previous step was obtained using a split window algorithm Eq. (5).

$$LSE = \varepsilon_s \times \left(1 - FVC\right) + \varepsilon_V \times FVC \quad (5)$$

ε_S: Emissivity of soil

FVC: Fractional vegetation cover

ε_V : Emissivity of vegetation

The surface emissivity image estimation requires the level of ε_V and ε_S of bands 10 and 11. Table 1.

Table 1. indicates the ε_V and ε_S

Emissivity coefficient	Band 10	Band 11
ε_S	**0.977**	**0.971**
ε_V	**0.989**	**0.987**

Considering Table 1. The value of soil and vegetation emissivity for bands 10 and 11 are very close to each other.

Still, the maximum value of surface emissivity is related to vegetation emissivity of the 11th band.

2.3.6. Average Combination of Surface LSE Image

The average combination of surface LSE images of bands 10 and 11 was computed using Eq. (7) and the LSE difference was calculated using Eq. (6,7).

$$\text{Mean of LSE} = m = \frac{LSE10 + LSE11}{2} \quad (6)$$

$$\text{The difference of LSE} = \Delta m = LSE10 - LSE11 \quad (7)$$

2.3.7. Split-Window Algorithm for LST

The proposed Split-Window algorithm utilizes the atmospheric window in the range of 10 μm to 12 μm wavelengths for the TIRS bands (10 and 11) (Feng et al., 2018). The basis of the split window algorithm is the radiance attenuation for atmospheric absorption, which is proportional to the radiance differences of simultaneous measurements at two different wavelengths, each of them being subject to various atmospheric absorption, LST was calculated using Equ. (8) (Rongali, Keshari, Gosain & Khosa, 2018).

$$\begin{aligned} LST &= TB_{10} + C1\left(TB_{10} - TB_{11}\right) \\ &+ C2\left(TB_{10} - TB_{11}\right)^2 + C0 \\ &+ \left(C3 + C4W\right)\left(1 - m\right) \\ &+ \left(C5 + C6W\right)\Delta m \end{aligned} \quad (8)$$

LST: Land Surface Temperature in kelvin

C: Split window coefficient values

TB: Spectral radiance of bands 10 and 11 in kelvin

W: Atmospheric water vapor content

m: Mean LSE of the TIRS bands

Δm : LSE difference

Table 2. Split window coefficient values

C0	**0.268**
C1	**1.378**
C2	**0.183**
C3	**54.300**
C4	**2.238**
C5	**129.2**
C6	**16.4**

2.3.8. Separation of Regions into Urban and Suburban Areas

In this study, Segmentation of urban and sub-urban areas for 20 chosen regions in the world was done through the following steps: (Zhou, Bonafoni, Zhang & Wang, 2018).

2.3.8.1. Building Pixels

Building pixels of Landsat 8 images were separated using Support Vector Machine (SVM), and for algorithm training purposes, the training regions were chosen using google earth.

2.3.8.2. The Density of Building Areas

After the identification of building pixels, for separation of urban and sub-urban areas, a 33 * 33 kernel was used that swept the whole image and the number of building pixels in the kernel was counted. The density of building areas was calculated using Eq. (9).

$$Density\left(i, j\right) = \frac{N}{M} \quad (9)$$

N: Number of building pixels in the kernel

M: The maximum number of building pixels in the kernel and the whole image

2.3.8.3. Separation of Urban and Suburban Areas

In this stage, the urban and suburban areas were separated. Due to the calculated density image of each region, two thresholds were selected as follows:

a) Density >0.5 the region is known as the urban area

b) 0.25< Density <0.5 the region is known as a suburban area

The MNDWI index was used to remove water pixels using Eq. (10).

$$MNDWI = \frac{Green - SWIR1}{Green + SWIR1} \quad (10)$$

2.3.9. Spectral Indices Calculation

To consider the effect of spectral indices on the SUHI phenomenon, the most influential spectral indices on this phenomenon, such as vegetation, moisture, building, were calculated (Renard, Alonso, Fitts, Hadjiosif & Comboy, 2019) (Ogashawar & Bastos 2012).

Table 3. Spectral Indices

Vegetation Cover spectral indices	
Normalized Difference Vegetation Index	(1)
$NDVI = \frac{NIR - RED}{NIR + RED}$	
Soil Adjusted Vegetation Index	(2)
$SAVI = \frac{NIR - RED}{NIR + RED + L} \times (L + 1)$	
Enhanced Vegetation Index	(3)
$EVI = G \times \frac{NIR - RED}{NIR + C_1 \times RED - C_2 \times BLUE + L}$	
Green Vegetation Index	(4)
$GVI = -0.2848 Blue - 0.2435 Green - 0.5436 Red + 0.7243 NearInfrared + 0.0840 Swir1 - 0.1800 Swir2$	
Moisture spectral indices	
Normalized Difference Moisture Index	(5)
$NDMI = \frac{NIR - SWIR1}{NIR + SWIR1}$	
Tasseled Cap-Wetness	(6)
$TCW = 0.1509 Blue + 0.197 Green + 0.3279 Red + 0.3406 NearInfrared - 0.7112 Swir1 - 0.4572 Swir2$	
Building spectral indices	
Normalized Difference Built-Up Index	(7)
$NDBI = \frac{SWIR1 - NIR}{NIR + SWIR1}$	
Urban Index	(8)
$UI = \frac{SWIR - NIR}{NIR + SWIR2}$	
Index-based Built-Up Index	(9)
$IBI = \frac{NDBI - \frac{(SAVI + MNDWI)}{2}}{NDBI + \frac{(SAVI + MNDWI)}{2}}$	

2.3.10. SUHI Calculation

The SUHI is referred to as heat pattern by surface characteristics consideration. SUHI is a reliable component to indicate atmospheric urban heat islands. The classical approach for analyzing the intensity of SUHI is the temperature difference between urban and suburban areas (Morabito et al., 2018), (Feng et al., 2019). However, the disparity between urban and rural areas remains a challenging issue (Renard et al., 2019). In the conceptual model, rural areas are defined as parts of an urban area that are not affected. Hence, the distinction between urban and rural areas is the result of SUHI analysis (Zhou et al.,2019). However, remote sensing studies often include a priori definition of "urban" versus "rural" regions with due attention to land cover. The SUHI can be calculated by Eq. (11).

SUHI = average of urban temperature an average of sub-urban temperature (11)

3. Evaluation and Results

Figure 3(A) shows the Building pixels of Landsat 8 images which were used in the classification of building regions of Amsterdam using the SVM algorithm (SVM), Figure 3(B) indicates the density of the building areas of Amsterdam, and Figure 3(C) illustrates the segmentation of urban and sub-urban areas of Amsterdam.

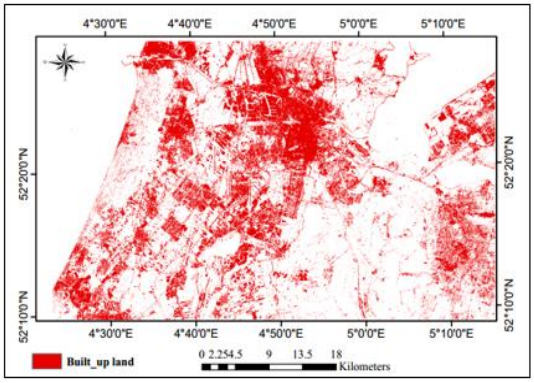

(A)

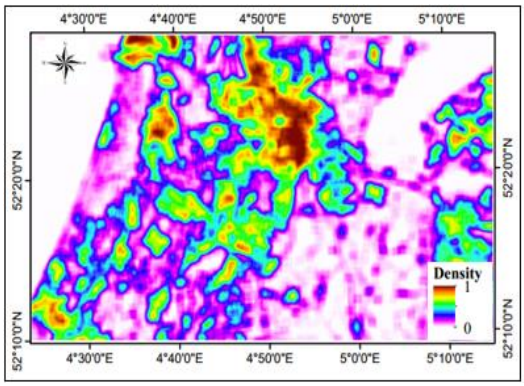

(B)

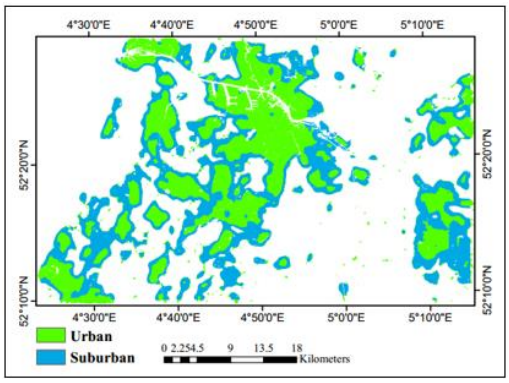

(C)

Figure 3. Separation of regions into urban and sub-urban areas of Amsterdam

According to the results, heat island shows different behavior in different climate types. In this study, it is attempted to evaluate at least one region for each kind of climate. To consider the factors that affect heat islands, different spectral indices such as vegetation, moisture, soil, and building index were used to identify these factors. The results are achieved as follows:

- **Amsterdam:** The daytime SUHI is positive and higher than the nighttime SUHI during the time of the study. By area temperature decrement, the daytime SUHI reduced and the nighttime SUHI increased. All of these are positive.

- **Baghdad:** The SUHI values are different during daytime; As the temperature of the area decreases, the SUHI changes from positive to negative, but its nighttime value is positive for both times with little difference.

- **Boston:** By the area temperature increment, the night and the daytime SUHI decreased. The SUHI values are positive for both times.

- **Brazil:** As the area's temperature increases, the SUHI slightly decreases for both times of day and night.

- **Chicago:** As the area's temperature increases, the daytime SUHI increases and the nighttime SUHI decreases. The SUHI values are positive for both day and nighttimes.

- **Dallas:** As the area's temperature increases, the SUHI decreases for both the night and daytime SUHI. The SUHI values are positive for both times of the day and night.

- **Istanbul:** As the area's temperature increases, the SUHI increases for both night and daytimes. SUHI values are positive for both times.

- **Heyderabad:** As the temperature increases, the daytime SUHI decreases, and the nighttime SUHI increases. The SUHI values are negative for both times of daytime SUHI and positive for nighttime SUHI.

- **Isfahan:** As the area's temperature increases, the daytime SUHI decreases, and the nighttime SUHI increases. Both daytime SUHI is negative and both nighttime SUHI is positive.

- **Lhasa:** As the area's temperature increases, the day and the nighttime SUHI increase too. The SUHI values are negative for both daytimes SUHIs and positive for nighttime SUHI.

- **Liverpool:** As the area's temperature increases, the daytime SUHI decreases, and the nighttime SUHI increases. The SUHI values are positive for both times.

- **Medina:** As the area's temperature increases, the day and the nighttime SUHI decreases. Both daytime SUHIs are negative and both nighttime SUHIs are positive.

- **Manama:** As the area's temperature increases, the daytime SUHI increases and the nighttime SUHI decreases. The SUHI values are positive for both times.

- **Niamey:** As the area's temperature increases, the day and the nighttime SUHIs decrease. The SUHI values are positive for both times.

- **Novosibirsk:** As the area's temperature increases, the day and the nighttime SUHI increase. The SUHI values are positive for both times.

- **Paris:** As the area's temperature increases, the day and the nighttime SUHI increase too. The SUHI values are positive for both times.

- **Perth:** As the area's temperature increases, the day and the nighttime SUHI decreases. The SUHI values are positive for both times.

- **San Francisco:** As the area's temperature increases, the daytime SUHI increases and the nighttime SUHI decreases. The SUHI values are positive for both times.

- **Tripoli:** As the area's temperature increases, the daytime SUHI increases and the nighttime SUHI decreases. The SUHI values are positive for both times.

- **Wuhan:** As the area's temperature increases, the daytime SUHI increases and the nighttime SUHI decreases. The SUHI values are positive for both times of day and night.

The night and day TIRS maps and the urban and non-urban segmentation for three regions including Paris, Hyderabad, and Manama are as follows:

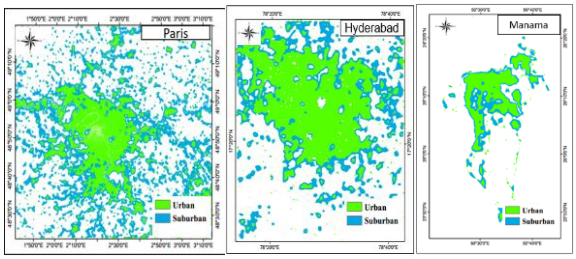

Figure 4. the image segmentation into urban and suburban areas of Paris, Heyderabad, Manama regions

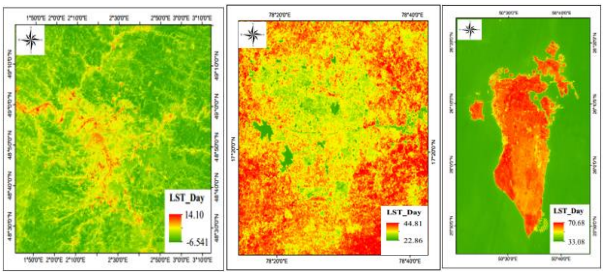

Figure 5. Daytime Land surface temperature of Paris, Heyderabad, Manama regions using Landsat 8 in summer

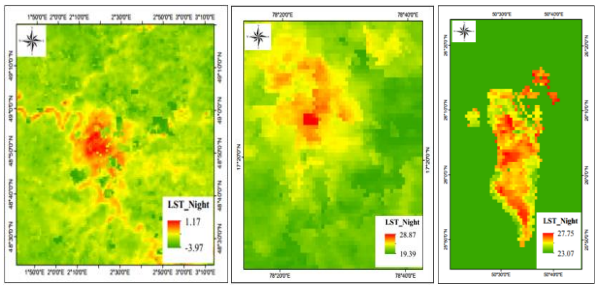

Figure 6. Nighttime Land surface temperature of Paris, Heyderabad, Manama regions using MODIS in summer

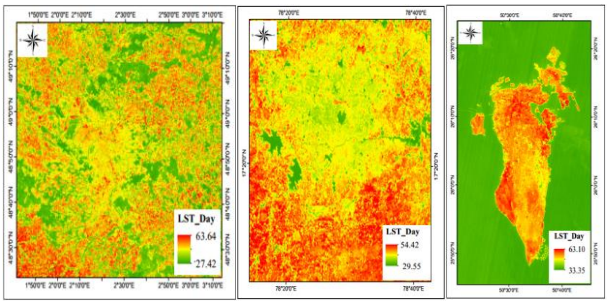

Figure 7. Daytime Land surface temperature of Paris, Heyderabad, Manama regions using Landsat 8 in winter

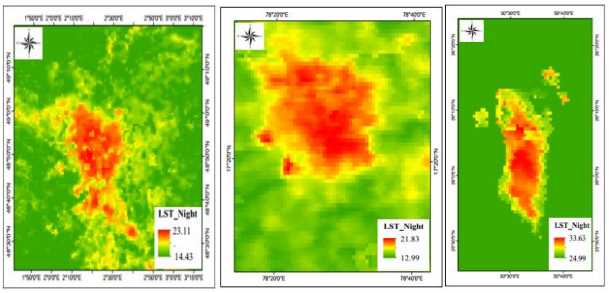

Figure 8. Nighttime Land surface temperature of Paris, Heyderabad, Manama regions using MODIS in winter

Day and Nighttime LST and SUHI average of case studies in winter and summer are as follows:

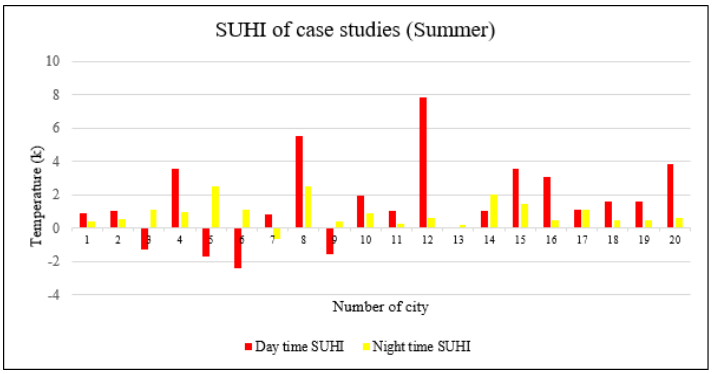

Figure 9. Average of Day and Nighttime LST and SUHI in summer

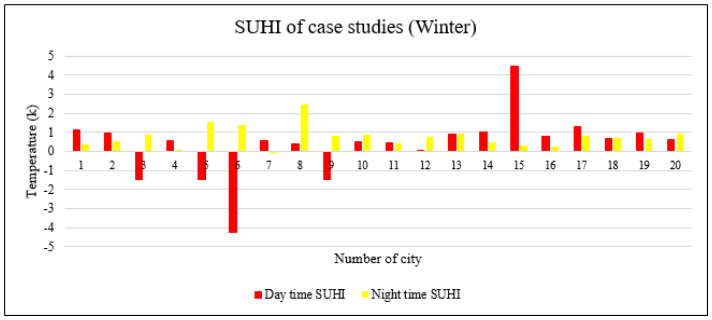

Figure 10. Average of Day and Nighttime LST and SUHI in winter

Regarding Figure 9 and Figure 10, the lowest amount of daytime SUHI refers to Isfahan during winter with moderate dry weather, and the highest amount of daytime SUHI refers to Tripoli during summer, with semi arid weather. The lowest amount of nighttime SUHI is observed in Manama during winter with dry weather and the highest amount of nighttime SUHI is observed in Baghdad during winter with warm and dry weather.

Based on the region's climate type, the temporal pattern of SUHI is divided into three positive and negative categories. The results are shown in Figure 11.

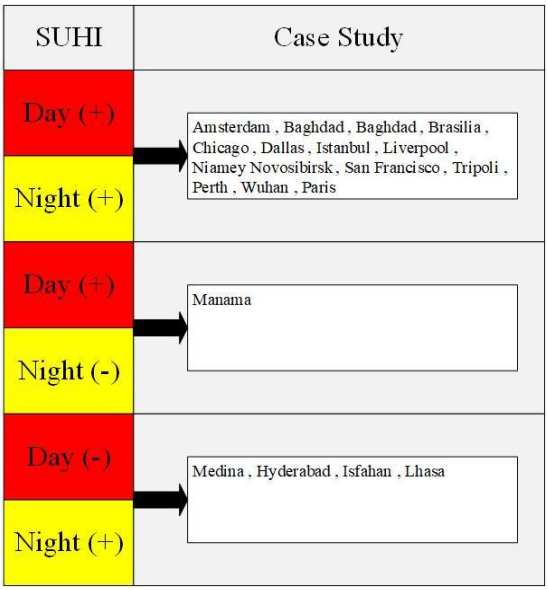

Figure 11. the temporal pattern of SUHI

According to the results, in arid and desert regions such as Isfahan, Hyderabad, Lhasa, and Medina, daytime urban area's temperature is lower than the surrounding area and the SUHI is negative, and vice versa, the nighttime temperature of the urban area is much higher than the surrounding area and the SUHI is positive. For temperate, humid, and Mediterranean regions, due to the presence of the river, the lake, or the sea around the urban areas such as Istanbul or Amsterdam, the day and the nighttime heat island is positive and higher than their surrounding area. Finally, only for Manama, the daytime heat island is higher than the surrounding area, and the nighttime shows a contrasting result.

The results of heat island values for 20 case studies indicate that the heat island values are different for each region. Still, for a specific region, the heat island has the same behavior. That means the positive or negative amount of night or daytime SUHI remains consistent with seasonal changes. For instance, the daytime SUHI of Manama is positive and the nighttime SUHI of Manama is negative. This behavior is uniform for different seasons and only the obtained amounts are different.

3.1. Correlation of SUHI and the Spectral Indices

A correlation coefficient is a tool for the determination of the type and the degree of relationships between two quantitative variables. The correlation coefficient is a criterion used to determine the association between two variables. This coefficient shows the relationship intensity as well as the type of relationship (direct or inverse). This index is always between 1 to 1 while a zero amount shows the absence of a relationship between the two variables.

The correlation between two random variables X and Y is defined by following Eq (12):

$$corr\left(X,Y\right)=\frac{\mathrm{cov}\left(X,Y\right)}{\sigma_X\,\sigma_Y} \qquad (12)$$

Cov: covariance

Corr: the usual symbol of the Pearson correlation

σ : The standard deviation symbol

The correlation coefficient between 0 to 1 means a positive correlation, and the closer the value to one means the stronger correlation. If the correlation coefficient of two parameters is positive, this means that in that study area, the increment of a parameter increases another parameter and the decrement of a parameter decreases another one. If the correlation coefficient of two parameters is negative, this means that in that study area, the increment of one parameter decreases another one and the decrement of one parameter increases another one. The zero correlation coefficient means that the two parameters in the study area are independent of each other and according to reduction or increment of one, decrease or increase of the other cannot be determined. The difference between spectral indices of urban and sub-urban areas and SUHI, their correlation coefficients are shown in Table 4.

Table 4. The correlation between indices and the SUHI

Kind of Spectral index	Name of Spectral index	Correlation coefficient
Vegetation	NDVI	-0.693
Vegetation	SAVI	-0.774
Vegetation	EVI	-0.738
Vegetation	GVI	-0.823
Moisture	NDMI	-0.736
Moisture	TCW	-0.611
Building	UI	0.723
Building	IBI	0.761
Building	NDBI	0.701

The positive values of the correlation coefficient indicate that by the increment of index values, the SUHI is also increasing too. The negative values of the correlation coefficient indicate that by increasing the index value, the SUHI will decrease too. According to Table 9, four vegetation indices and two moisture indices have negative correlation coefficients, which means that by the vegetation cover and moisture increment, the SUHI will be decreased. Also, the bare soil and the building spectral indices have positive correlation coefficients, which indicates that by the increment of these spectral indices, the SUHI will be increased. From the vegetation indices, the GVI index has the maximum value of correlation than other vegetation

indices. The NDMI index had a higher correlation coefficient than the TCW index. The IBI index had a higher correlation coefficient than other building indices as illustrated in Figure 12.

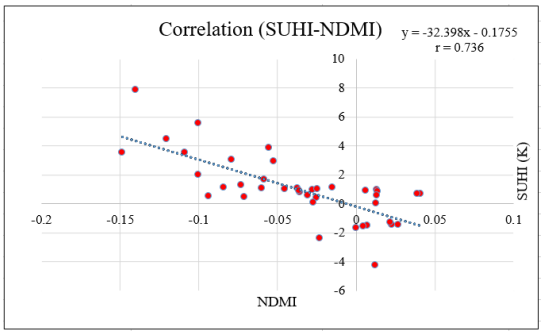

(A)

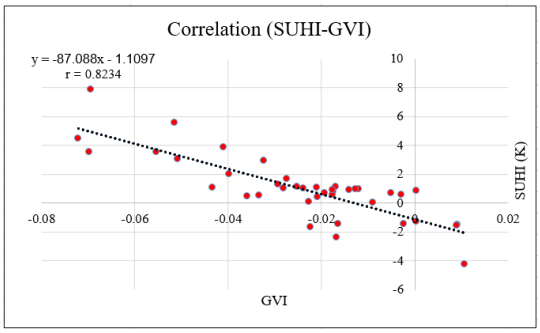

(B)

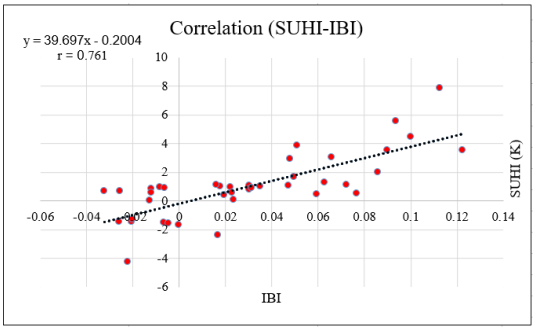

(C)

Figure 12. Correlation of SUHI and the spectral indices

4. Conclusion

Heat island is one of the environmental issues that could have a destructive impact on urban communities. Nowadays, a considerable number of studies are being done on this phenomenon and many of them are based on satellite data. Nevertheless, the study results have shown that heat island phenomena are growing rapidly and have affected many crowded cities. Heat island has different spatial and temporal patterns that could be different from one region to another.

This study was aimed to find out some temporal and spatial patterns of this phenomenon. For this purpose, 20 different regions over the world were selected and their day and nighttime SUHI for two different dates of a year were calculated using Landsat 8 and MODIS data. Several spectral indices such as vegetation, moisture, building, and bare soil indices were also calculated using Landsat data for case studies. The results showed that the SUHI could have different values for day, night, and also different days of a year. However, for most of the regions with a temperate and Mediterranean climate, the SUHI has positive values for both day and night. Moreover, for warm, dry, and desert areas the daytime SUHI has negative values and the nighttime SUHI has positive values. According to 20 case studies, only Manama that is a warm and dry city, the nighttime SUHI was negative and the daytime SUHI was positive. The positive or negative values of SUHI have remained constant over a year. For the subsequent studies, to find more accurate spatial and temporal patterns, it could be suggested to construct their research on a higher number of case studies. Some factors, such as wind level and wind direction, can also be considered.

References

Azevedo, J. A., Chapman, L., & Muller, C. L. (2016). Quantifying the daytime and night-time urban heat island in Birmingham, UK: A comparison of satellite-derived land surface temperature and high-resolution air temperature observations. *Remote Sensing*, *8* .١٥٣ ,(٢)

Benas, N., Chrysoulakis, N., & Cartalis, C. (2017). Trends of urban surface temperature and heat island characteristics in the Mediterranean. *Theoretical and Applied Climatology*, *130*(3-4), 807-816.

Debbage, N., & Shepherd, J. M. (2015). The urban heat island effect and city contiguity. *Computers, Environment and Urban Systems*, *54*, 181-194.

Feng, Y., Gao, C., Tong, X., Chen, S., Lei, Z., & Wang, J. (2019). Spatial patterns of land surface temperature and their influencing factors: a case study in Suzhou, China. *Remote Sensing*, *11*(2), 182.

Feng, Y., Li, H., Tong, X., Chen, L., & Liu, Y. (2018). Projection of land surface temperature considering the effects of future land change in the Taihu Lake Basin of China. *Global and Planetary Change*, *167* .٣٤-٢٤ ,

Ferguson, B., Fisher, K., Golden, J., Hair, L., Haselbach, L., Hitchcock, D., . . . Waye, D. (2008). Reducing urban heat islands: Compendium of strategies-cool pavements.

He, J., Zhao, W., Li, A., Wen, F., & Yu, D. (2019). The impact of the terrain effect on land surface temperature variation based on Landsat-8 observations in mountainous areas. *International journal of remote sensing*, *40*(5-6), 1808-1827.

Kalnay, E., & Cai, M. (2003). Impact of urbanization and land-use change on climate. *Nature*, *423*(6939), 528-531.

Koken, P. J., Piver, W. T., Ye, F., Elixhauser, A., Olsen, L. M., & Portier, C. J. (2003). Temperature, air pollution, and hospitalization for cardiovascular diseases among elderly people in Denver. *Environmental health perspectives*, *111*(10), 1312-1317.

Lin, P., Lau, S. S. Y., Qin, H., & Gou, Z. (2017). Effects of urban planning indicators on urban heat island: a case study of pocket parks in a high-rise high-density environment. *Landscape and Urban Planning, 168*, 48-60.

Meng, Q., Zhang, L., Sun, Z., Meng, F., Wang, L., & Sun, Y. (2018). Characterizing spatial and temporal trends of surface urban heat island effect in an urban main built-up area: A 12-year case study in Beijing, China. *Remote Sensing of Environment, 204*, 826-837.

Morabito, M., Crisci, A., Georgiadis, T., Orlandini, S., Munafò, M., Congedo, L., . . . Zazzi, M. (2018). Urban imperviousness effects on summer surface temperatures nearby residential buildings in different urban zones of Parma. *Remote Sensing, 10*(1), 2 .٦

Ogashawara, I., & Bastos, V. d. S. B. (2012). A quantitative approach for analyzing the relationship between urban heat islands and land cover. *Remote Sensing, 4*(11), 3596-3618.

Renard, F., Alonso, L., Fitts, Y., Hadjiosif, A., & Comby, J. (2019). Evaluation of the effect of urban redevelopment on surface urban heat islands. *Remote Sensing, 11*(3), 299.

Rizwan, A. M., Dennis, L. Y., & Chunho, L. (2008). A review on the generation, determination, and mitigation of Urban Heat Island. *Journal of Environmental Sciences, 20*(1), 120-128.

Rongali, G., Keshari, A. K., Gosain, A. K., & Khosa, R. (2018). Split-window algorithm for retrieval of land surface temperature using Landsat 8 thermal infrared data. *Journal of Geovisualization and Spatial Analysis, 2*(2) .١٤ ,

Schatz, J., & Kucharik, C. J. (2014). Seasonality of the urban heat island effect in Madison, Wisconsin. *Journal of Applied Meteorology and Climatology, 53*(10), 2371-2386.

Sobrino, J. A., Oltra-Carrió, R., Sòria, G., Jiménez-Muñoz, J. C., Franch, B., Hidalgo, V., . . . Romaguera, M. (2013). Evaluation of the surface urban heat island effect in the city of Madrid by thermal remote sensing. *International journal of remote sensing, 34*(9-10), 3177-3192.

Wang, J., Zhan, Q., & Guo, H. (2016). The morphology, dynamics, and potential hotspots of land surface temperature at a local scale in urban areas. *Remote Sensing, 8*(1), 18.

Wu, Z., & Zhang, Y. (2018). Spatial variation of urban thermal environment and its relation to green space patterns: Implication to sustainable landscape planning. *Sustainability, 10*(7), 2249.

Xian, G., & Crane, M. (2006). An analysis of urban thermal characteristics and associated land cover in Tampa Bay and Las Vegas using Landsat satellite data. *Remote Sensing of Environment,* ١٤٧- ,(٢)١٠٤ .١٥٦

Zhou, D., Bonafoni, S., Zhang, L., & Wang, R. (2018). Remote sensing of the urban heat island effect in a highly populated urban agglomeration area in East China. *Science of the Total Environment, 628*, 415-429.

Zhou, D., Xiao, J., Bonafoni, S., Berger, C., Deilami, K., Zhou, Y., . . . Sobrino, J. A. (2019). Satellite remote sensing of surface urban heat islands: progress, challenges, and perspectives. *Remote Sensing, 11*(1), 48.